Cell Reports

Resource

Selective Laminin-Directed Differentiation of Human Induced Pluripotent Stem Cells into Distinct Ocular Lineages

Graphical Abstract

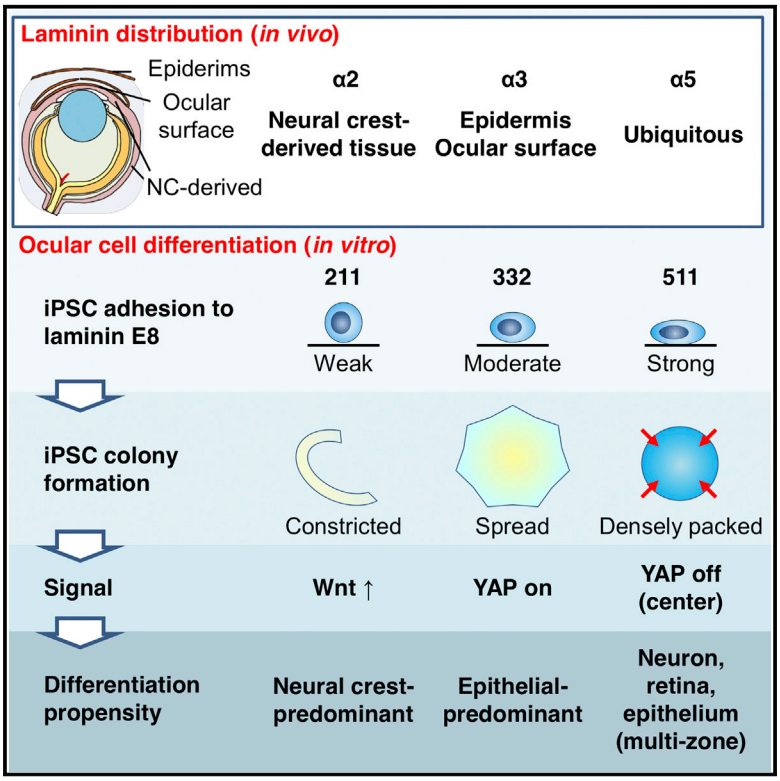

Highlights

- LN211E8 promotes hiPSC differentiation into neural crest cells via Wnt activation
- LN332E8 promotes hiPSC differentiation into corneal epithelial cells
- LN511E8 led to YAP inactivation and retinal differentiation in hiPSC colony centers
- Distributions of laminins in the developmental eye mirrored the hiPSC type it induced

Authors

Shun Shibata, Ryuhei Hayashi, Toru Okubo, ..., Andrew J. Quantock, Kiyotoshi Sekiguchi, Kohji Nishida

Correspondence

ryuhei.hayashi@ophthal.med.osaka-u.ac.jp (R.H.), knishida@ophthal.med.osaka-u.ac.jp (K.N.)

In Brief

Shibata *et al.* report that laminin isoforms differentially regulate the ocular cell differentiation from hiPSCs. The binding affinity of laminin and integrins determines the nature of expanded hiPSC colonies in terms of cell motility, cell-cell interactions, and cell density, with the involvement of Wnt and YAP signals.

Shibata et al., 2018, Cell Reports *25*, 1668–1679
November 6, 2018
https://doi.org/10.1016/j.celrep.2018.10.032

CellPress

OPEN ACCESS
CellPress

Cell Reports
Resource

Selective Laminin-Directed Differentiation of Human Induced Pluripotent Stem Cells into Distinct Ocular Lineages

Shun Shibata,[1,2] Ryuhei Hayashi,[1,3,6,*] Toru Okubo,[1,2] Yuji Kudo,[1,2] Tomohiko Katayama,[3] Yuki Ishikawa,[3] Junko Toga,[4] Emiko Yagi,[4] Yoichi Honma,[1,2] Andrew J. Quantock,[5] Kiyotoshi Sekiguchi,[4] and Kohji Nishida[3,*]

[1]Department of Stem Cells and Applied Medicine, Osaka University Graduate School of Medicine, Suita, Osaka 565-0871, Japan
[2]Research and Development Division, ROHTO Pharmaceutical Co., Ltd., Osaka, Osaka 544-8666, Japan
[3]Department of Ophthalmology, Osaka University Graduate School of Medicine, Suita, Osaka 565-0871, Japan
[4]Division of Matrixome Research and Application, Institute for Protein Research, Osaka University, Suita, Osaka 565-0871, Japan
[5]Structural Biophysics Group, School of Optometry and Vision Sciences, College of Biomedical and Life Sciences, Cardiff University, Cardiff CF24 4HQ, Wales, UK
[6]Lead Contact
*Correspondence: ryuhei.hayashi@ophthal.med.osaka-u.ac.jp (R.H.), knishida@ophthal.med.osaka-u.ac.jp (K.N.)
https://doi.org/10.1016/j.celrep.2018.10.032

SUMMARY

The extracellular matrix plays a key role in stem cell maintenance, expansion, and differentiation. Laminin, a basement membrane protein, is a widely used substrate for cell culture including the growth of human induced pluripotent stem cells (hiPSCs). Here, we show that different isoforms of laminin lead to the selective differentiation of hiPSCs into different eye-like tissues. Specifically, the 211 isoform of the E8 fragment of laminin (LN211E8) promotes differentiation into neural crest cells via Wnt activation, whereas LN332E8 promotes differentiation into corneal epithelial cells. The immunohistochemical distributions of these laminin isoforms in the developing mouse eye mirrors the hiPSC type that was induced *in vitro*. Moreover, LN511E8 enables generation of dense hiPSC colonies due to actomyosin contraction, which in turn led to cell density-dependent YAP inactivation and subsequent retinal differentiation in colony centers. Thus, distinct laminin isoforms determine the fate of expanded hiPSCs into eye-like tissues.

INTRODUCTION

Human pluripotent stem cells (hPSCs), including human embryonic stem cells (hESCs) and human induced pluripotent stem cells (hiPSCs), can undergo long-term expansion in culture and be induced to differentiate into cells of all three germ layers (Takahashi et al., 2007; Thomson et al., 1998; Yu et al., 2007). As such, they have considerable value for developmental studies, drug screening, and research in regenerative medicine. Soluble components in the culture medium, including growth factors, provide cues for hPSC fate specification, as do culture substrates and their coating with extracellular matrix (ECM) proteins (Czyz and Wobus, 2001; Hayashi and Furue, 2016). The ECM plays a fundamental role in the maintenance of the stem cell niche, as it regulates the proliferation and differentiation of stem cells (Gattazzo et al., 2014). The ECM protein laminin, a major component of basement membranes, is a heterotrimeric protein assembled from α (α1–5), β (β1–3), and γ (γ1–3) chain subunits, the composition of which is reflected in the isoform nomenclature (Aumailley et al., 2005). The expression of laminin is spatiotemporally regulated, especially during development (Miner et al., 1997; Nguyen and Senior, 2006), with several laminin isoforms able to support hPSC proliferation in undifferentiated states (Miyazaki et al., 2008; Rodin et al., 2010, 2014; Xu et al., 2001). Truncated versions of the protein—the laminin E8 fragments (LNE8)—permit robust proliferation of hPSCs (Miyazaki et al., 2012), while other isoforms are known to be effective in the long-term expansion or generation of specific somatic cell types from hPSCs (Fusaoka-Nishioka et al., 2011; Kanninen et al., 2016; Ohta et al., 2016; Takayama et al., 2013, 2016).

Using E8 fragments of laminin-511 (LN511E8), we have generated hiPSC-derived colonies comprising four concentric cell zones, the emergence of which displays some similarities with ocular development (Hayashi et al., 2016, 2017). We termed these types of colonies "self-formed ectodermal autonomous multi-zones" (SEAMs) of eye-like cells. SEAMs grown on LN511E8 contain cells with the immunostaining characteristics of different ocular lineages, and include retinal-like cells, lens-like cells, and cells reminiscent of ocular surface epithelial cells. Here, we differentiated hiPSCs on a range of laminin isoforms and show that the nature of the laminin isoform is instrumental in the determination of cell fate.

RESULTS

Laminin Isoform-Dependent Autonomous Differentiation of hiPSCs

When coated onto culture plates, five isoforms of LNE8 (111, 211, 332, 411, and 511) were each able to support autonomous differentiation of hiPSC clones 201B7 and 1383D2. Although cell

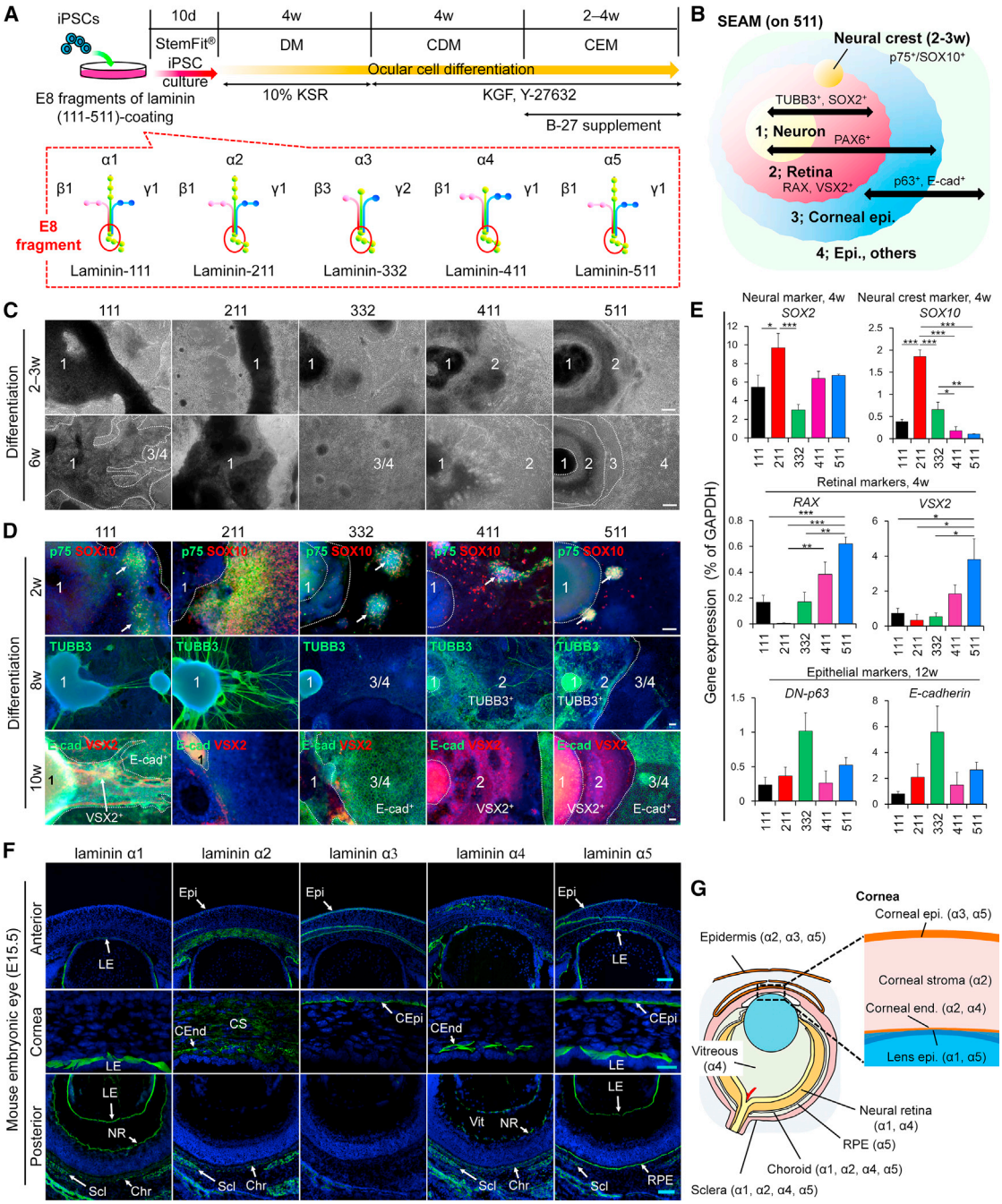

Figure 1. Ocular Cell Differentiation from hiPSCs on Different Laminin Isoforms

(A) Schematic representation of the ocular cell differentiation protocol on laminin isoforms.

(B) SEAM structure on LN511E8.

(C) Phase contrast images of hiPSCs grown on different laminin isoforms. Scale bars: 200 μm. The numbers indicate SEAM zones to which the differentiated cells correspond.

(D) Immunostaining of cells differentiated on different laminin isoforms: p75 (green) and SOX10 (red) were stained after 2 weeks of differentiation, TUBB3 (green) after 8 weeks of differentiation, and E-cadherin (green) and VSX2 (red) after 10 weeks of differentiation. Nuclei, blue. Scale bars: 100 μm.

(E) Gene expression analysis in cells differentiated on each laminin isoform. Neural, neural crest, retinal, and epithelial markers were analyzed at 4, 4, 4, and 12 weeks of differentiation, respectively. The results are presented as means ± SEM; n = 5 cell samples of three independent experiments for 111, 332, 411, and 511; n = 4 cell samples of three independent experiments for 211 (neural, neural crest, and retinal markers); and n = 3 cell samples of two independent experiments for all isoforms (epithelial markers). *p < 0.05, **p < 0.01, and ***p < 0.001.

(legend continued on next page)

Table 1. An Indication of Zonal Formation on Different Laminin Isoforms and Distributions of Laminin Isoforms during Mouse Eye Development

Ocular Cell Differentiation from hiPSCs[a]						
		E8 Fragments of Laminin				
Cell type	Zone	111	211	332	411	511
Neural crest (2–4w)	2	+	++	+	+	+
Retina	2	–	–	–	+	+
Epithelium	3	–	+	++	–	+
Mouse Embryonic Eye (E15.5)[b]						
Cell type		Laminin Expression				
		α1	α2	α3	α4	α5
Neural crest-derived		+ (Chr, Scl)	+ (CS, CEnd, Chr, Scl)	–	+ (CEnd, Chr, Scl, Vit)	+ (Scl)
Retina		+ (NR)	–	–	+ (NR)	+ (RPE)
Epithelium		+ (LE)	+ (Epi)	+ (Epi, CEpi)	–	+ (Epi, CEpi, LE)

[a]An indication of zonal formation on different laminin isoforms. (++), (+), and (–) indicate larger, equivalent, or lower amounts of zone formation than that observed on LN511E8, respectively.
[b]Epi, epidermis; CEpi, corneal epithelium; CS, corneal stroma; CEnd, corneal endothelium; LE, lens epithelium; Chr, Choroid; Scl, Sclera; Vit, Vitreous; NR, neuroretina; RPE, retinal pigment epithelium.

viability varied by isoform, in all cases cells adhered, proliferated, and expressed pluripotency markers (Figures 1A and S1A–S1D). The typical four-zone SEAM structure seen previously, however, was only generated in the presence of LN511E8, the isoform employed in our published experiments (Figure 1B) (Hayashi et al., 2016, 2017). The other four isoforms, LN111E8, LN211E8, LN332E8, and LN411E8, supported the formation of SEAMs with distinct structural configurations. As identified by their morphology under phase contrast microscopy, hiPSCs expanded on LN111E8 tended to aggregate and stratify and were composed mainly of zone 1 cells along with a minor component of zone 3/4 cells. When grown on LN211E8, the differentiated cells resembled those from LN511E8-cultured zone 1. Cells differentiated on LN332E8 gave rise exclusively to cells of SEAM zones 3 and 4, which display an epithelial-like phenotype. Cells differentiated on LN411E8 resembled those from LN511E8-cultured zones 1 and 2 (Figure 1C).

Analysis of eye development-related markers revealed that LN111E8 and LN211E8 led to the appearance of TUBB3$^+$ neuronal fibers. Moreover, LN211E8 promoted differentiation of p75$^+$/SOX10$^+$ presumed neural crest cells (Kim et al., 2003). We also confirmed that LN211E8 promoted differentiation of p75$^+$/ITGA4$^+$ cells (Bixby et al., 2002; Morrison et al., 2000; Pinco et al., 2001) by flow cytometry (Figure S2A). On the other hand, numerous E-cadherin$^+$ epithelial cells were present in colonies grown on LN332E8. When cultured on LN411E8, TUBB3$^+$ cells, which were confined to zone 2 in LN511E8-derived SEAMs, expanded more peripherally. Neuroretinal marker VSX2$^+$ cells (Meyer et al., 2009) were induced on both LN411E8- and LN511E8-coated dishes (Figure 1D). The gene expression levels of the neural marker *SOX2* and neural crest marker *SOX10* were relatively high in cells differentiated on LN211E8. In agreement with immunostaining results, the expression levels of retina-related genes, such as *RAX* and *VSX2*, were elevated in cells differentiated on LN411E8 and LN511E8, while those of the epithelial genes *DN-p63* and *E-cadherin* were high in cells differentiated on LN332E8 (Figures 1E and S2B).

The distribution of laminin in developing mammalian eyes has been the subject of previous investigations (Byström et al., 2006; Qin et al., 1997) and was examined in detail here. At embryonic day 15.5 (E15.5) in the mouse, expression of isoform α1 was confirmed in the lens epithelium, neuro-retina, choroid, and sclera. Isoform α2 was expressed in neural crest-derived tissues such as the corneal stroma, corneal endothelium, choroid, and sclera, while α3 was expressed in stratified epithelial cells of the epidermis and corneal epithelium. α4 was expressed in corneal endothelium, vitreous, neuroretina, choroid, and sclera. α5 was expressed in a range of epithelial tissues, including the epidermis, corneal epithelium, lens epithelium, retinal pigment epithelium (RPE), and sclera (Figures 1F and 1G). Collectively, these results indicated that distinct laminin isoforms differentially affect autonomous ectoderm cell differentiation in hiPSC culture. Moreover, it appears as though the laminin isoform associated with various ocular tissues in the developing eye *in vivo* can be employed *in vitro* to direct differentiation into this type of cell (Table 1).

Use of LN332E8 for Corneal Epithelial Sheet Fabrication from hiPSCs

Based on the results described above, we hypothesized that LN332E8 would be able to effectively facilitate the generation of hiPSC-derived corneal epithelial cells (iCECs). To investigate this, after 10–12 weeks of differentiation culture of hiPSCs on each laminin isoform, the percentage of SSEA-4$^+$/ITGB4$^+$/CD200$^-$ cells (i.e., the iCEC fraction) was evaluated by flow cytometry. This revealed that hiPSCs differentiated on LN332E8 possessed the highest proportion of iCECs (Figures 2A and 2B). Moreover, iCECs differentiated on this isoform (i.e., 332-iCECs) exhibited a colony-forming efficiency equivalent to that of iCECs differentiated on LN511E8 (511-iCECs) (Figures 2C–2E). The 332-iCECs and 511-iCECs, when expanded, formed a cell sheet that expressed the corneal epithelial markers PAX6, keratin (KRT) 12, p63, and MUC16 (Figure 2F). qRT-PCR analysis revealed no significant differences between expanded

(F) Immunostaining for laminin α1–5 (green) during mouse eye development at E15.5; similar data (not shown) were obtained at E18.5. Nuclei, blue. Scale bars: 100 μm (in anterior and posterior panels) and 20 μm (in cornea panels). Epi, epidermis; LE, lens epithelium; CEpi, corneal epithelium; CS, corneal stroma; CEnd, corneal endothelium; Chr, choroid; Scl, sclera; Vit, Vitreous; NR, neuroretina; RPE, retinal pigment epithelium.
(G) Schematic of mouse embryonic eye (E15.5) and expression of laminin α chains.

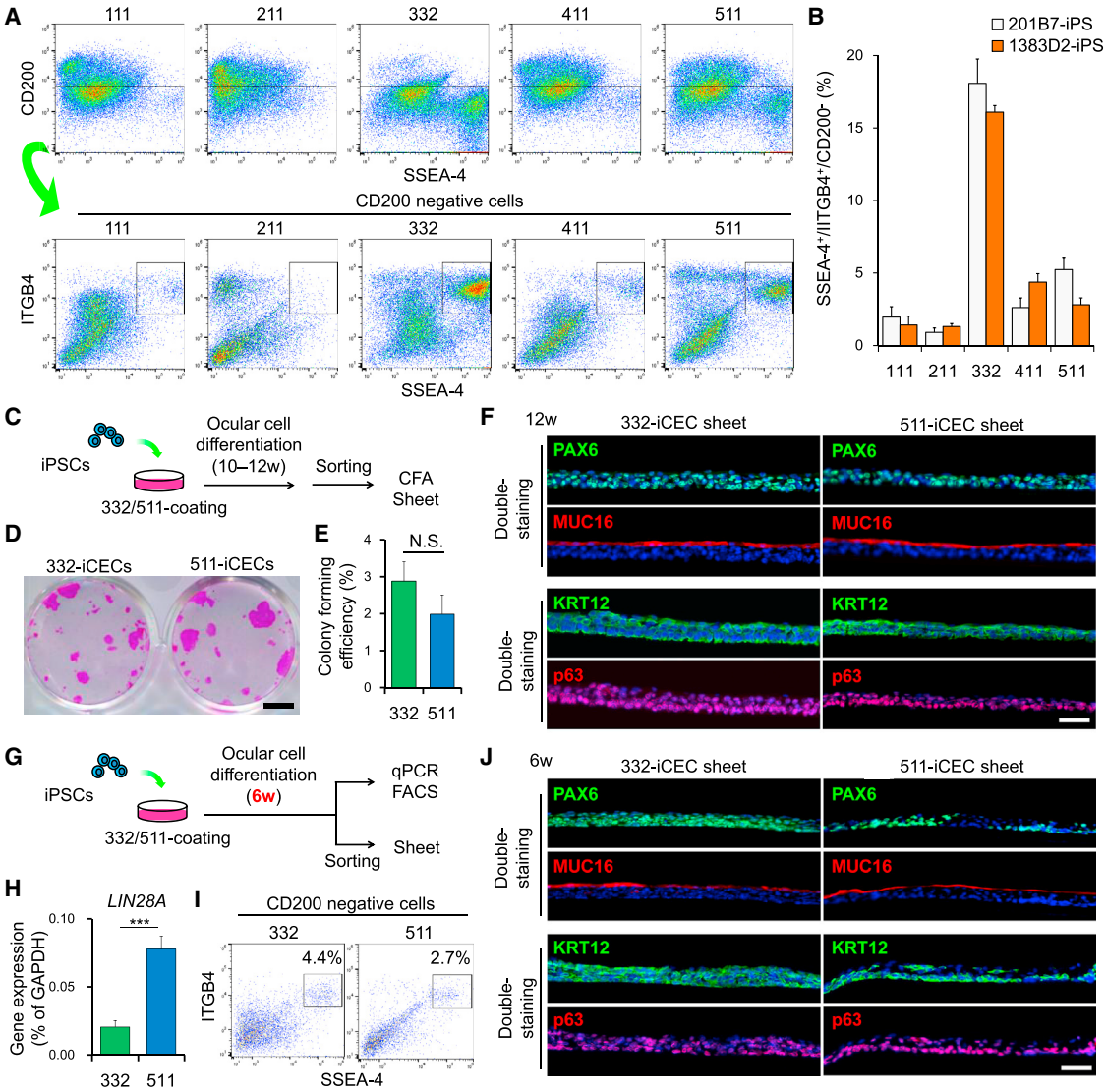

Figure 2. LN332E8 for iCEC Fabrication

(A) Flow cytometry analysis for SSEA-4$^+$/ITGB4$^+$/CD200$^-$ cells after 10–12 weeks of differentiation culture. Live cells were analyzed using antibodies specific for SSEA-4 and CD200 (upper panel). CD200$^-$ cells were analyzed using antibodies specific to SSEA-4 and ITGB4 (lower panel).

(B) Quantification of SSEA-4$^+$/ITGB4$^+$/CD200$^-$ cells in differentiated 201B7 and 1383D2 cells (mean ± SEM; n = 13 for 111 and 411, n = 9 cell samples for 211, n = 20 cell samples for 332 and 511 [201B7], 13 independent experiments; n = 4 samples of two independent experiments for all isoforms [1383D2]).

(C) Schematic of differentiation protocol.

(D and E) Colony-forming assays for 332-iCECs and 511-iCECs. Fixed colonies were stained with Rhodamine B (D) and colony-forming efficiency was calculated (E). The results are presented as means ± SEM; n = 7 cell samples of two independent experiments. Scale bar: 5 mm.

(F) Immunostaining for PAX6 (green), MUC16 (red), KRT12 (green), and p63 (red) in 332-iCEC and 511-iCEC sheets at 12 weeks. Nuclei, blue. Scale bar: 50 μm.

(G) Schematic of differentiation protocol.

(H) Gene expression analysis for *LIN28A* in differentiated hiPSCs on LN332E8 and LN511E8 at 6 weeks of differentiation. The results are presented as means ± SEM; n = 6 cell samples of three independent experiments; ***p < 0.001.

(I) Flow cytometry graphs for SSEA-4$^+$/ITGB4$^+$/CD200$^-$ cells after 6 weeks of differentiation culture (mean values from three independent experiments).

(J) Immunostaining for PAX6 (green), MUC16 (red), KRT12 (green), and p63 (red) in stratified 332-iCEC and 511-iCEC sheets at 6 weeks. Nuclei, blue. Scale bar: 50 μm.

332-iCEC and 511-iCEC sheets in the expression levels of genes encoding corneal and non-corneal epithelial markers (Figure S3A).

Based on the heightened efficiency of the LN332E8 substrate in the generation of iCEC sheets, we investigated the possibility of using an abridged (i.e., 6-week) cultivation period (Figure 2G). This revealed that cultivation on LN332E8 resulted in reduced expression of *LIN28A*, a marker of residual undifferentiated cells, compared to the expression in cells cultured on LN511E8 (Figure 2H). Cells grown on LN332E8 also produced higher numbers

of SSEA-4$^+$/ITGB4$^+$/CD200$^-$ cells than those cultivated on LN511E8 (Figure 2I), while the 332-iCEC-generated sheet exhibited strong expression of corneal epithelial markers. The cell sheet prepared using 511-iCECs, in contrast, was inadequate in this regard (Figure 2J), indicating that LN332E8 is effective in enhancing the yield of iCECs and shortening the differentiation period for iCEC sheet preparation. It was also notable that SEAM zone 1 cells (corresponding to neural cells) proliferate slowly when cultured on LN332E8 and easily detach from the substrate after long-term differentiation (Figures S3B–S3D).

Wnt Activation on LN211E8 during Neural Crest Differentiation

Microarray analysis, hierarchical clustering, and principal-component analysis of differentially expressed genes in hiPSCs during the early stage (i.e., day 3) of differentiation on each laminin isoform showed that cultivation on LN211E8, LN332E8, and LN511E8 resulted in marked changes in gene expression (Figures 3A–3D, S4A, and S4B). We further analyzed differentially upregulated genes in cells on each isoform using WikiPathways (Table S1). The number of pathways with a p value less than 0.05 was greatest on 211. In agreement with the results shown in Figure 2, in the 211 pathway list, the pathway with the lowest p value was "neural crest differentiation" ($p = 1.05 \times 10^{-8}$) (Table S1). LN211E8 induced neural crest development-related genes even at this early phase of differentiation (Figure 3E). Furthermore, cells differentiated on LN211E8 expressed PITX2 and FOXC1, craniofacial neural crest markers (Figure 3F). We also found that the "Wnt signaling pathway" was enriched (fifth lower, $p = 5.87 \times 10^{-4}$) in upregulated genes in cells differentiated on LN211E8 (Table S1). Figures 3G and S4C show the Wnt signaling pathway-related genes. We confirmed that expression of the Wnt/β-catenin target genes *AXIN2* and *LEF1* was upregulated in the cells cultured on LN211E8 (Figure 3H).

Wnt activation is known to elicit the differentiation of hPSCs into neural crest cells (Leung et al., 2016; Menendez et al., 2011). To examine this, we treated hiPSCs grown on LN211E8 or LN511E8 with IWP2, a Wnt signaling inhibitor, or CHIR99021, a Wnt signaling agonist, for the first 3 days of differentiation (Figure 3I). After 2 weeks of differentiation, 49% and 0.39% of the cells grown on LN211E8 and LN511E8, respectively, were p75$^+$/ITGA4$^+$ presumed neural crest cells. Notably, treatment with the Wnt inhibitor IWP2 decreased the proportion of p75$^+$/ITGA4$^+$ cells on LN211E8 by 12%. In contrast, the Wnt activator CHIR99021 promoted the emergence of p75$^+$/ITGA4$^+$ cells on LN511E8 by 7.6% (Figure 3J). Immunostaining analysis detected a decrease in p75$^+$/SOX10$^+$ cells on LN211E8 following IWP2 treatment and an increase in these cells on LN511E8 after CHIR99021 treatment (Figure 3K). These findings indicate that LN211E8-activated Wnt signaling is necessary for the commitment of hPSCs to become neural crest cells.

Cell Density-Dependent Inactivation of YAP within hiPSC Colonies on LN511E8

When examining hiPSCs using time-lapse microscopy, it became evident that hiPSC colony formation on LN332E8 occurred via cells proliferating and migrating outward, whereas cells on LN511E8 proliferated with little radial movement (Figure 4A). Colonies grown on LN332E8 grew to a larger final size than those grown on LN511E8, but at a more gradual pace (Figures 4B and 4C). The relative lack of cell movement in LN511E8-expanded hiPSC colonies resulted in a comparatively high cell density toward the centers of these colonies (Figures 4D and 4E). In these cell-dense central regions of LN511E8-expanded colonies, N-cadherin was highly expressed after 3 days of differentiation (Figure 4F), suggesting that cell density may be instrumental in neuroectoderm differentiation at the center of the colonies cultured on this isoform. Moreover, microarray analysis suggested that genes involved in the specialization of the retina, such as *RAX*, *PAX6*, *LHX2*, and *MAB21L2* (Bailey et al., 2004), were upregulated in hiPSCs grown on LN511E8 compared to those cultured on LN332E8 (Figure S4D).

YAP is a transcription factor that senses cell density and regulates neuronal specifications (Hsiao et al., 2016). Here, we uncovered a correlation between the expression levels of cytoplasmic YAP and PAX6 in differentiated hiPSCs grown on both LN332E8 and LN511E8 at day 3 of differentiation. Cytoplasmic YAP localization and PAX6 expression were higher in the cells grown on LN511E8 than in those grown on LN332E8 (Figure 4G). Cell fractionation followed by western blotting also showed that the proportion of nuclear YAP was higher in cells cultivated on LN332E than in cells grown on LN511E8 (Figure 4H). The expression levels of YAP target genes, including *CTGF* and *CYR61*, were downregulated in hiPSCs cultured on LN511E8-coated dishes compared to levels observed in cells cultured on LN332E8-coated dishes after 10 days in iPSC culture (Figure 4I).

To ascertain whether cell density causes YAP inactivation, we examined the relationship between hiPSC density and neuroectoderm differentiation. This revealed that YAP inactivation and neuroectoderm differentiation were promoted by increasing cell seeding numbers (Figure S5A) and the duration of the colony forming period (Figures 4J–4L and S5B). It also became apparent that the levels of F-actin, which are known to affect YAP activity (Sansores-Garcia et al., 2011), did not differ between cells cultured on LN332E8 or LN511E8 (Figure S5C). To investigate whether YAP activity regulates differentiation, we treated hiPSCs with verteporfin (VP), a suppressor of the YAP-TEAD interaction (Liu-Chittenden et al., 2012) and found that it resulted in enhanced expression of *PAX6* and *RAX* (Figures 4M and S5D). Similarly, *PAX6* and *RAX* expression was increased in the presence of latrunculin A (Lat-A), an inhibitor of F-actin that is necessary for YAP nuclear localization (Figures S5E–S5G). Together, these results clearly demonstrate that culturing hiPSCs on LN511E8 leads to YAP inactivation and neuroectoderm differentiation at the center of hiPSC-derived colonies and that high cell density is a key factor in this process.

Actomyosin Contraction for Dense hiPSC Colony Formation on LN511E8

Phosphorylated myosin light chain (p-MLC), a contractile force marker, was strongly localized at the periphery of hiPSC colonies, especially those grown on LN511E8 (Figure 5A). Western blot analysis showed that MLC phosphorylation was stimulated in hiPSCs cultivated on LN511E8, but inhibited in those cultivated on LN211E8. On day 10, p-MLC was also observed in hiPSC colonies grown on LN332E8. In contrast, cells cultivated

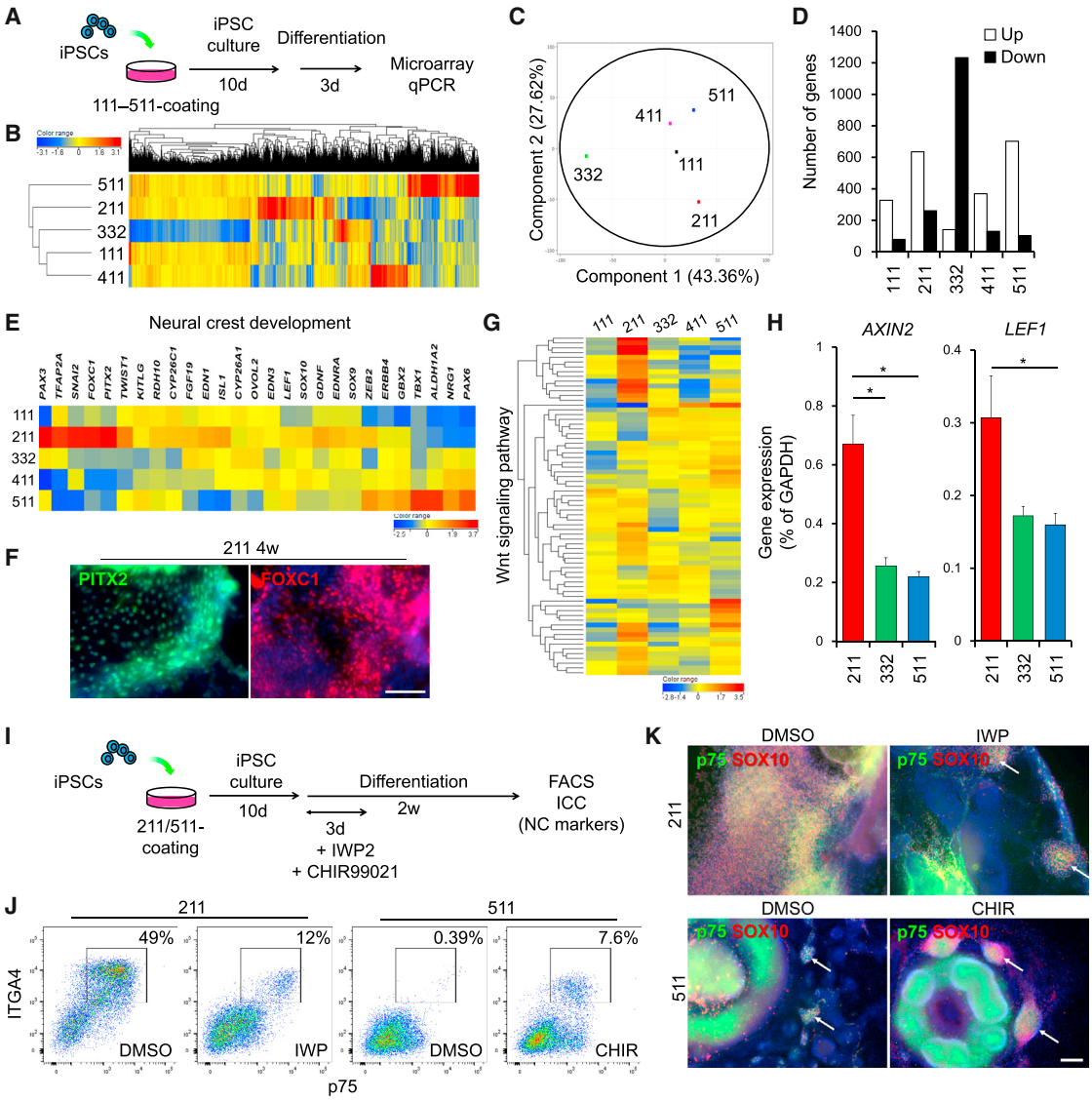

Figure 3. LN211E8 Activates Wnt Signaling and Neural Crest Differentiation in hiPSCs

(A) Schematic of differentiation protocol.

(B) Hierarchical cluster analysis of differentially expressed genes using Euclidean distance and complete linkage metric.

(C) Principal-component analysis of differentially expressed genes.

(D) The number of upregulated and downregulated genes in cells differentiated on each isoform.

(E) Heatmap of gene expression levels for neural crest development-related genes in cells differentiated on different laminin isoforms.

(F) Immunostaining for PITX2 (green) and FOXC1 (red) in cells differentiated on LN211E8 at 4 weeks of differentiation. Nuclei, blue. Scale bar: 100 μm.

(G) Hierarchical cluster analysis of Wnt signaling pathway-related genes in cells differentiated on different laminin isoforms.

(H) Gene expression analysis of Wnt/β-catenin target genes in cells differentiated on LN211E8, LN332E8, and LN511E8 after 3-day differentiation culture. The results are presented as means ± SEM; n = 5 cell samples of two independent experiments; *p < 0.05.

(I) Schematic of differentiation protocol. ICC, immunocytochemistry; NC, neural crest.

(J) Flow cytometry graph for p75 and ITGA4 in cells differentiated on LN211E8 with or without IWP2 (5 μM) and on LN511E8 with or without CHIR99021 (10 μM) (mean values from three independent experiments).

(K) Immunostaining for p75 (green) and SOX10 (red) in cells differentiated on LN211E8 with or without IWP2 (5 μM) and on LN511E8 with or without CHIR99021 (10 μM). The arrows indicate $p75^{+}/SOX10^{+}$ cells. Nuclei, blue. Scale bar: 100 μm.

on LN211E8 exhibited enhanced phosphorylation of vinculin, which recognizes cell-cell but not cell-matrix adhesions (Bays et al., 2014), as determined using antibody Y822 (Figure 5B). Thus, it was suggested that cell-cell interactions and cell-matrix interactions predominate on LN211E8 and LN511E8, respectively (Figure 5C). Based on this reasoning, we tested the premise that the coating concentration of LN511E8 would affect iPSC behavior and subsequent differentiation. Indeed, when

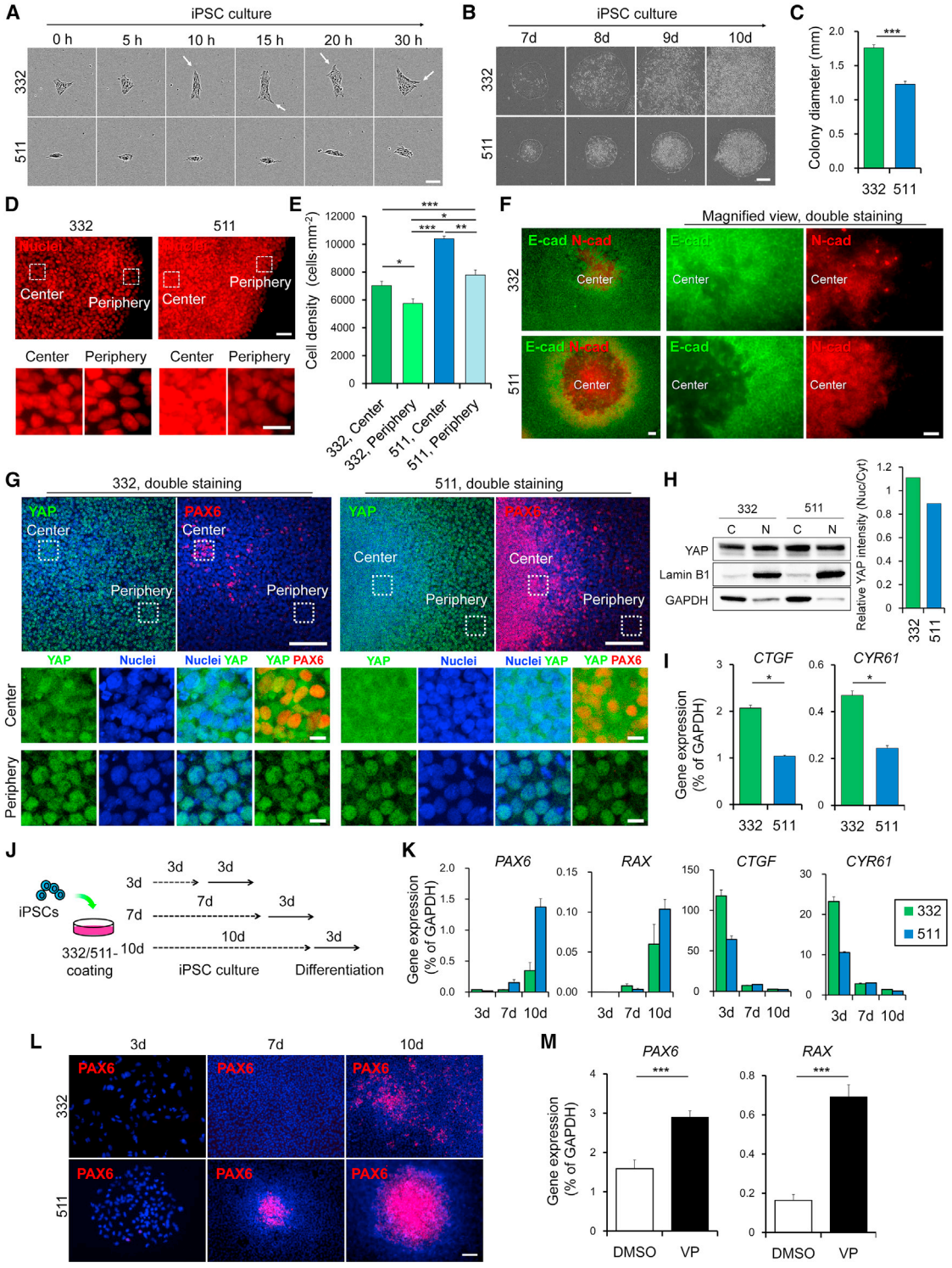

Figure 4. Cell Density-Dependent YAP Inactivation within hiPSC Colonies on LN511E8

(A and B) Time-lapse microscopy of hiPSCs on LN332E8 and LN511E8 at early stage (A) and late stage (B) of iPSC culture. Scale bars: 100 μm (A) and 300 μm (B). In (A), the observation starting point (0 hr) was after 2 days in culture.

(C) Diameters of hiPSC colonies at day 10 of iPSC culture are presented as means ± SEM; n = 10 colonies; ***$p < 0.001$.

(D) Cells at the center and periphery of hiPSC colonies on LN332E8 and LN511E8. Nuclei, red. Scale bars: 50 μm (upper) and 20 μm (lower magnified panels).

(E) Quantification of cell densities are shown as means ± SEM; n = 10 colonies; *$p < 0.05$, **$p < 0.01$, and ***$p < 0.001$.

(legend continued on next page)

the coating concentration of LN511E8 was increased, focal adhesions recognized by vinculin were formed, and the shape of the colonies became more rounded (Figure 5D). Furthermore, p-MLC levels at the periphery of hiPSC colonies, PAX6 expression, and colony compaction were also found to positively correlate with LN511E8 coating concentrations (Figures 5E–5G and S6). These results suggest that LN511E8 promotes actomyosin contraction through the strength and frequency of adhesion within hiPSC colonies (Figure 5H). Indeed, treatment with blebbistatin, a myosin heavy chain ATPase inhibitor (Straight et al., 2003), abolished hiPSC compaction during colony formation and resulted in a reduced cell density (Figures 5I–5L). This led to decreased PAX6 expression and YAP nuclear localization (Figure 5M), as confirmed by qRT-PCR analysis, which revealed a reduction in *PAX6* and *RAX* expression (and an increase in *CTGF* and *CYR61* expression) following pre-treatment with blebbistatin (Figure 5N). Cumulative evidence thus points to the actomyosin contractile force as a driver of the formation of densely packed central regions of hiPSC colonies grown on LN511E8, which, in turn, likely promotes YAP inactivation and subsequent neuroectoderm differentiation.

DISCUSSION

The microenvironment surrounding stem cells, including the identity of ECM proteins and growth factors and the physical characteristics of the supporting tissue, are all important for determining stem cell fates (Engler et al., 2006; Kundu and Putnam, 2006; Pryzhkova et al., 2014). We previously developed the "SEAM method" using LN511E8, which can preferentially induce ocular cell lineages including corneal, retinal, and neural crest cells, mimicking *in vivo* eye development. This method is considered to be suitable for examining the relationship between eye development and substrates. Here, we show how a typical SEAM containing four concentric cell zones was formed only when hiPSCs were grown on LN511E8. When cells were expanded on LN211E8 or LN332E8, on the other hand, the formation of neural crest cells and epithelial cells (including the corneal epithelium) was induced, respectively.

Our analysis of the distribution of laminin isoforms in developing mammalian eyes (Figure 1) suggests that the particular eye tissue with which a specific laminin isoform is associated *in situ* is also the one to which the isoform tends to give rise *in vitro*. This raises the possibility of selecting an appropriate isoform for target hiPSC culture. Consistent with this, we found an increase in hiPSC-derived corneal epithelial differentiation using LN332E8, the E8 fragment of laminin-332 expressed specifically in the stratified epithelium (Figure 2). In our published method of SEAM formation from hiPSCs grown on LN511E8, it was necessary to pipette away cells other than the epithelial-like cells from the SEAM to efficiently harvest sufficient numbers of remaining cells to allow their expansion into an iCEC sheet. Such an intervention is not ideal, however, as it requires some experience, and the outcome is not always reproducible or favorable. Culturing hiPSCs on LN332E8, however, eliminates this pipetting step, and, although the use of this substrate does not induce the expansion of neural-like cells (Figures S2B–S2D), it appreciably shortens the culture period for iCEC sheet production. Therefore, the use of LN332E8 for hiPSC expansion can be recommended for the fabrication of iCEC sheets.

hPSCs mainly express integrin $\alpha6\beta1$ (Miyazaki et al., 2008, 2012), which has a particularly high affinity for laminin-511 but low affinity for laminin-211 (Nishiuchi et al., 2006; Yamada and Sekiguchi, 2015). hiPSCs differentiated on LN211E8 in the current experiments were characterized by high expression of neural crest-related markers and genes encoding Wnt pathway proteins and their targets (Figure 3). Canonical Wnt signaling plays a critical role in neural crest induction *in vivo* (García-Castro et al., 2002) and *in vitro* (Menendez et al., 2011). Accordingly, we showed that inhibition of Wnt signaling decreased neural crest cell differentiation from hiPSCs. Wnt inhibition during hESC differentiation has been shown to occur on stiff substrates due to the degradation of β-catenin via integrin β1-dependent GSK3 and Src activity (Przybyla et al., 2016). As mentioned above, LN211E8 has the lowest affinity for integrin $\alpha6\beta1$; thus, it seems likely that substrates with low affinity for hiPSCs lead to Wnt activation upon initiation of differentiation.

Our data revealed that YAP also plays an important role in determining the fates of hPSCs. YAP is an effector of the Hippo pathway, which is integral for contact inhibition, organ size restriction, and mechanotransduction (Dupont et al., 2011; Zhao et al., 2007). YAP is also involved in the long-term survival and expansion of hPSCs (Ohgushi et al., 2015), and its inhibition on soft substrata promotes differentiation into neural lineages (Dupont, 2016; Musah et al., 2014; Sun et al., 2014). A recent report also indicated that the extent of YAP inactivation, which depends on cell density, prompts hPSCs to differentiate into neuroepithelial cells (Hsiao et al., 2016). Consistent with these

(F) Immunostaining for E-cadherin (green) and N-cadherin (red) in cells on LN332E8 and LN511E8 at day 3 of differentiation culture. Scale bars: 100 μm (left) and 50 μm (right, magnified panels).
(G) Immunostaining for YAP (green) and PAX6 (red) in hiPSCs on LN332E8 and LN511E8 at day 3 of differentiation. Nuclei, blue. Scale bars: 50 μm (upper) and 100 μm (lower magnified panels).
(H) hiPSCs on LN332E8 and LN511E8 were fractionated and analyzed by western blotting (left). Nuclear YAP intensity relative to cytoplasmic YAP was quantified (right). C, cytoplasmic fraction; N, nuclear fraction.
(I) Gene expression in hiPSCs on LN332E8 and LN511E8 at day 10 of iPSC culture. Results are shown as means ± SEM; n = 4 cell samples of two independent experiments; *$p < 0.05$.
(J) Schematic of differentiation protocol.
(K) Gene expression in cells. The results are presented as means ± SEM; n = 4 cell samples of two independent experiments.
(L) Immunostaining for PAX6 (red) in cells. Nuclei, blue. Scale bar: 100 μm.
(M) Gene expression in hiPSCs on LN511E8 with or without verteporfin (VP) (0.3 μM) at day 3 of differentiation culture. Results are shown as means ± SEM; n = 3 cell samples; ***$p < 0.001$.

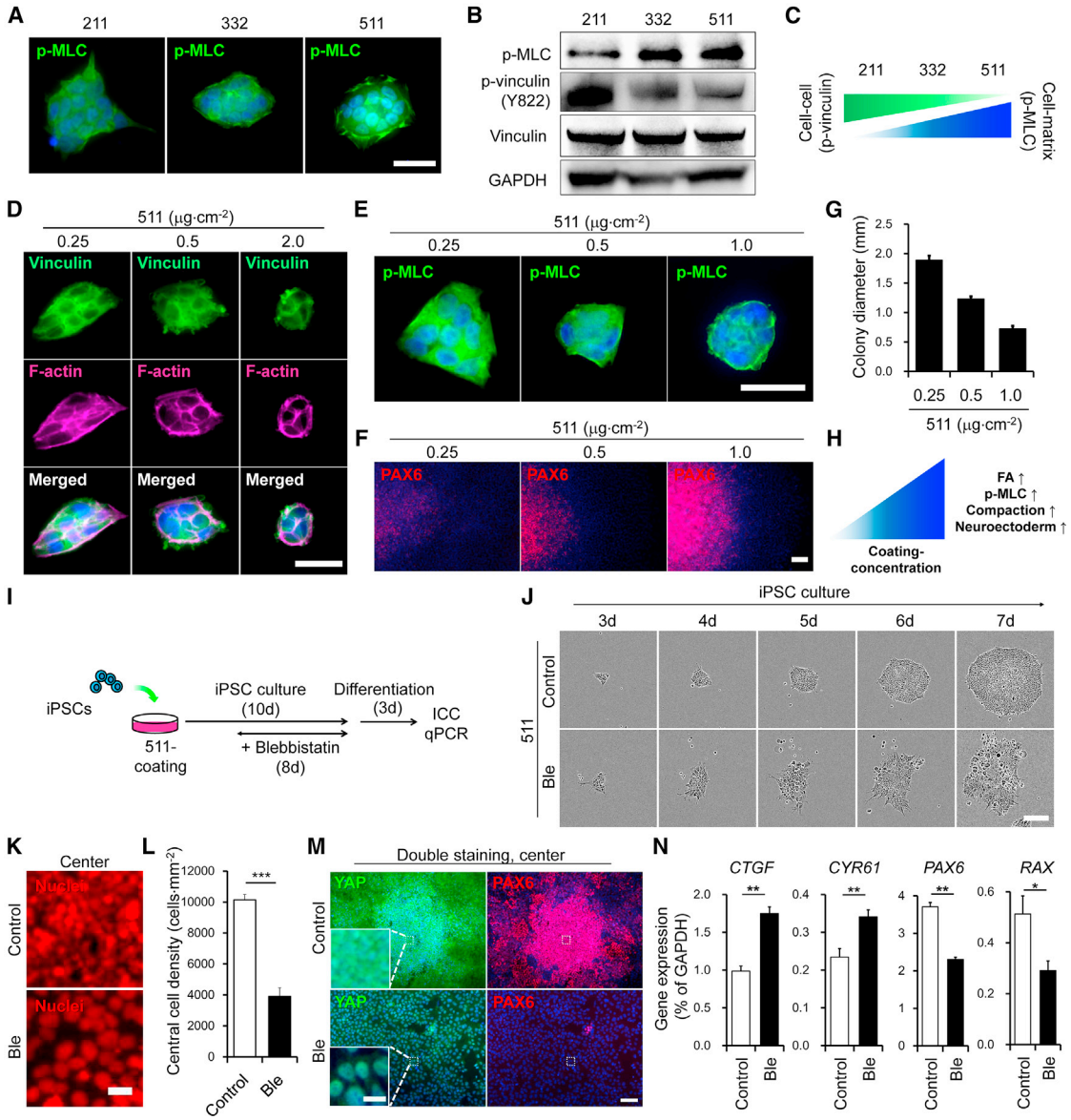

Figure 5. Actomyosin Contraction and Dense Packing of hiPSCs Grown on LN511E8

(A) Immunostaining for p-MLC (green) in hiPSCs on LN211E8, LN332E8, and LN511E8. Nuclei, blue. Scale bar: 50 μm.

(B) hiPSCs on LN211E8, LN332E8, and LN511E8 analyzed by western blotting.

(C) Schematic of dominant interactions.

(D) Immunostaining for vinculin (green) and phalloidin staining for F-actin (magenta) in hiPSCs on LN511E8 (0.25–2.0 $\mu g \cdot cm^{-2}$). Nuclei, blue. Scale bar: 50 μm.

(E) Immunostaining for p-MLC (green) in hiPSCs on LN511E8 (0.25–1.0 $\mu g \cdot cm^{-2}$). Nuclei, blue. Scale bar: 50 μm.

(F) Immunostaining for PAX6 (red) in cells on day 3 of differentiation culture. Nuclei, blue. Scale bar: 100 μm.

(G) Diameter of hiPSC colonies on LN511E8 at different concentrations at day 10. The results are shown as means ± SEM; n = 10 colonies.

(H) The effects of LN511E8.

(I) Schematic of experimental method.

(J) Time-lapse microscopy of hiPSC on LN511E8 with or without blebbistatin (5 μM, Ble). Scale bar: 200 μm.

(K) Representative images of cells. Nuclei, red. Scale bar: 20 μm.

(L) Quantification of cell densities are presented as means ± SEM; n = 9 colonies; ***$p < 0.001$.

(M) Immunostaining for YAP (green) and PAX6 (red) in cells at the center of hiPSC colonies on LN511E8 at day 3 of differentiation. Nuclei, blue. Scale bars: 100 μm and 20 μm (magnified panels).

(N) Gene expression in hiPSCs on LN511E8 with or without blebbistatin. Results are shown as means ± SEM; n = 7 cell samples of two independent experiments; *$p < 0.05$ and **$p < 0.01$.

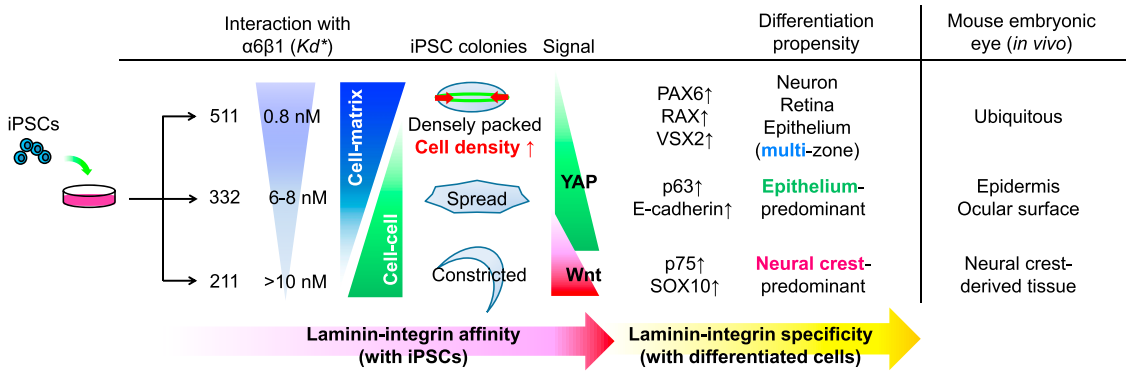

Figure 6. Schematic of Mechanism How the Laminin Isoforms Determine hiPSC Status and Fate
For the affinity of laminin-α6β1, see the report by Nishiuchi et al. (2006).

data, we found that neuroectodermal markers, such as PAX6, are expressed at the centers of high-cell-density hiPSC colonies grown on LN511E8. In these cells, YAP was excluded from the nucleus, and its inactivation was most likely due to high cell density (Figures 4 and S5). We also showed that actomyosin contraction is involved in the compaction of hiPSC colonies cultured on LN511E8 and confirmed that MLC phosphorylation, dense colony packing, and neuroectoderm differentiation of hiPSCs increased proportionally with the concentration of LN511E8 coating (Figure 5). This is in line with the findings of Toh et al. (2015), who reported that activated myosin II, localized to the periphery of hPSC colonies on Matrigel, is attenuated by treatment with an anti-α6β1 antibody. Thus, the strength and frequency of integrin α6β1-substrate binding promotes actomyosin contraction at the periphery of hPSC colonies. LN511E8 has a stronger affinity for α6β1 than other substrates, such as Matrigel (Miyazaki et al., 2012), thus allowing the establishment of densely packed hPSC colonies achieved via actomyosin contraction and accompanied by central neuroectodermal differentiation.

Collectively, the data presented here demonstrate that ectodermal differentiation from hiPSCs can be modulated by the informed selection of the laminin isoform used as a substrate. Moreover, we have shown that the binding affinity of substrates and integrins determines the nature of expanded hiPSC colonies in terms of cell motility, cell-cell interactions, and cell density, with the clear involvement of Wnt and YAP signals. The difference in affinity between differentiated cells and laminin isoforms thus, we contend, controls the manner in which cells spread and what proportion become ectodermal cells (Figure 6). This information helps elucidate the mechanism of SEAM formation on LN511E8, which has a unique arrangement consisting of the neuroectoderm in the central region of the colony and surface ectoderm at the periphery. It also provides a laminin isoform-mediated selective differentiation method for hiPSC expansion, differentiation, and fate.

STAR★METHODS

Detailed methods are provided in the online version of this paper and include the following:

SUPPLEMENTAL INFORMATION

Supplemental Information includes six figures and two tables and can be found with this article online at https://doi.org/10.1016/j.celrep.2018.10.032.

ACKNOWLEDGMENTS

We would like to thank S. Hara, H. Takayanagi, S. Araki, Y. Taniwaki, Y. Yamate, R. Katori, Y. Yasukawa, Y. Kobayashi, A. Honda, and E. Kimura of Osaka University for their technical assistance. This work was supported in part by the project for the realization of regenerative medicine of the Japan Agency for Medical Research and Development (AMED) and Grant-in-Aid for Scientific Research (S) (17K11480) from the Japan Society for the Promotion of Science (JSPS).

AUTHOR CONTRIBUTIONS

S.S., R.H., K.S., and K.N. designed the research. S.S., T.O., Y.K., T.K., and Y.I. designed and performed experiments and analyzed data. J.T., E.Y., and K.S. produced and provided reagents (LNE8s and anti-mouse laminin α antibodies). Y.H. and K.S. supervised the project. S.S., A.J.Q., and R.H. analyzed data and wrote the paper.

DECLARATION OF INTERESTS

S.S., T.O., Y.K., and Y.H. are employees of ROHTO Pharmaceutical Co., Ltd. R.H. is affiliated with the endowed chair of ROHTO Pharmaceutical Co., Ltd. K.S. is a co-founder and shareholder of Matrixome, Inc.

Received: March 14, 2018
Revised: September 10, 2018
Accepted: October 5, 2018
Published: November 6, 2018

REFERENCES

Aumailley, M., Bruckner-Tuderman, L., Carter, W.G., Deutzmann, R., Edgar, D., Ekblom, P., Engel, J., Engvall, E., Hohenester, E., Jones, J.C., et al. (2005). A simplified laminin nomenclature. Matrix Biol. *24*, 326–332.

Bailey, T.J., El-Hodiri, H., Zhang, L., Shah, R., Mathers, P.H., and Jamrich, M. (2004). Regulation of vertebrate eye development by Rx genes. Int. J. Dev. Biol. *48*, 761–770.

Bays, J.L., Peng, X., Tolbert, C.E., Guilluy, C., Angell, A.E., Pan, Y., Superfine, R., Burridge, K., and DeMali, K.A. (2014). Vinculin phosphorylation differentially regulates mechanotransduction at cell-cell and cell-matrix adhesions. J. Cell Biol. *205*, 251–263.

Bixby, S., Kruger, G.M., Mosher, J.T., Joseph, N.M., and Morrison, S.J. (2002). Cell-intrinsic differences between stem cells from different regions of the peripheral nervous system regulate the generation of neural diversity. Neuron *35*, 643–656.

Byström, B., Virtanen, I., Rousselle, P., Gullberg, D., and Pedrosa-Domellöf, F. (2006). Distribution of laminins in the developing human eye. Invest. Ophthalmol. Vis. Sci. *47*, 777–785.

Czyz, J., and Wobus, A. (2001). Embryonic stem cell differentiation: the role of extracellular factors. Differentiation *68*, 167–174.

Dupont, S. (2016). Role of YAP/TAZ in cell-matrix adhesion-mediated signalling and mechanotransduction. Exp. Cell Res. *343*, 42–53.

Dupont, S., Morsut, L., Aragona, M., Enzo, E., Giulitti, S., Cordenonsi, M., Zanconato, F., Le Digabel, J., Forcato, M., Bicciato, S., et al. (2011). Role of YAP/TAZ in mechanotransduction. Nature *474*, 179–183.

Engler, A.J., Sen, S., Sweeney, H.L., and Discher, D.E. (2006). Matrix elasticity directs stem cell lineage specification. Cell *126*, 677–689.

Fusaoka-Nishioka, E., Shimono, C., Taniguchi, Y., Togawa, A., Yamada, A., Inoue, E., Onodera, H., Sekiguchi, K., and Imai, T. (2011). Differential effects of laminin isoforms on axon and dendrite development in hippocampal neurons. Neurosci. Res. *71*, 421–426.

García-Castro, M.I., Marcelle, C., and Bronner-Fraser, M. (2002). Ectodermal Wnt function as a neural crest inducer. Science *297*, 848–851.

Gattazzo, F., Urciuolo, A., and Bonaldo, P. (2014). Extracellular matrix: a dynamic microenvironment for stem cell niche. Biochim. Biophys. Acta *1840*, 2506–2519.

Hayashi, Y., and Furue, M.K. (2016). Biological effects of culture substrates on human pluripotent stem cells. Stem Cells Int. *2016*, 5380560.

Hayashi, R., Ishikawa, Y., Sasamoto, Y., Katori, R., Nomura, N., Ichikawa, T., Araki, S., Soma, T., Kawasaki, S., Sekiguchi, K., et al. (2016). Co-ordinated ocular development from human iPS cells and recovery of corneal function. Nature *531*, 376–380.

Hayashi, R., Ishikawa, Y., Katori, R., Sasamoto, Y., Taniwaki, Y., Takayanagi, H., Tsujikawa, M., Sekiguchi, K., Quantock, A.J., and Nishida, K. (2017). Coordinated generation of multiple ocular-like cell lineages and fabrication of functional corneal epithelial cell sheets from human iPS cells. Nat. Protoc. *12*, 683–696.

Hsiao, C., Lampe, M., Nillasithanukroh, S., Han, W., Lian, X., and Palecek, S.P. (2016). Human pluripotent stem cell culture density modulates YAP signaling. Biotechnol. J. *11*, 662–675.

Ido, H., Harada, K., Futaki, S., Hayashi, Y., Nishiuchi, R., Natsuka, Y., Li, S., Wada, Y., Combs, A.C., Ervasti, J.M., and Sekiguchi, K. (2004). Molecular dissection of the alpha-dystroglycan- and integrin-binding sites within the globular domain of human laminin-10. J. Biol. Chem. *279*, 10946–10954.

Ido, H., Nakamura, A., Kobayashi, R., Ito, S., Li, S., Futaki, S., and Sekiguchi, K. (2007). The requirement of the glutamic acid residue at the third position from the carboxyl termini of the laminin gamma chains in integrin binding by laminins. J. Biol. Chem. *282*, 11144–11154.

Kanninen, L.K., Harjumäki, R., Peltoniemi, P., Bogacheva, M.S., Salmi, T., Porola, P., Niklander, J., Smutný, T., Urtti, A., Yliperttula, M.L., and Lou, Y.R. (2016). Laminin-511 and laminin-521-based matrices for efficient hepatic specification of human pluripotent stem cells. Biomaterials *103*, 86–100.

Kim, J., Lo, L., Dormand, E., and Anderson, D.J. (2003). SOX10 maintains multipotency and inhibits neuronal differentiation of neural crest stem cells. Neuron *38*, 17–31.

Kundu, A.K., and Putnam, A.J. (2006). Vitronectin and collagen I differentially regulate osteogenesis in mesenchymal stem cells. Biochem. Biophys. Res. Commun. *347*, 347–357.

Leung, A.W., Murdoch, B., Salem, A.F., Prasad, M.S., Gomez, G.A., and García-Castro, M.I. (2016). WNT/β-catenin signaling mediates human neural crest induction via a pre-neural border intermediate. Development *143*, 398–410.

Liu-Chittenden, Y., Huang, B., Shim, J.S., Chen, Q., Lee, S.J., Anders, R.A., Liu, J.O., and Pan, D. (2012). Genetic and pharmacological disruption of the TEAD-YAP complex suppresses the oncogenic activity of YAP. Genes Dev. *26*, 1300–1305.

Manabe, R., Tsutsui, K., Yamada, T., Kimura, M., Nakano, I., Shimono, C., Sanzen, N., Furutani, Y., Fukuda, T., Oguri, Y., et al. (2008). Transcriptome-based systematic identification of extracellular matrix proteins. Proc. Natl. Acad. Sci. USA *105*, 12849–12854.

Menendez, L., Yatskievych, T.A., Antin, P.B., and Dalton, S. (2011). Wnt signaling and a Smad pathway blockade direct the differentiation of human pluripotent stem cells to multipotent neural crest cells. Proc. Natl. Acad. Sci. USA *108*, 19240–19245.

Meyer, J.S., Shearer, R.L., Capowski, E.E., Wright, L.S., Wallace, K.A., McMillan, E.L., Zhang, S.C., and Gamm, D.M. (2009). Modeling early retinal development with human embryonic and induced pluripotent stem cells. Proc. Natl. Acad. Sci. USA *106*, 16698–16703.

Miner, J.H., Patton, B.L., Lentz, S.I., Gilbert, D.J., Snider, W.D., Jenkins, N.A., Copeland, N.G., and Sanes, J.R. (1997). The laminin alpha chains: expression, developmental transitions, and chromosomal locations of alpha1-5, identification of heterotrimeric laminins 8-11, and cloning of a novel alpha3 isoform. J. Cell Biol. *137*, 685–701.

Miyazaki, T., Futaki, S., Hasegawa, K., Kawasaki, M., Sanzen, N., Hayashi, M., Kawase, E., Sekiguchi, K., Nakatsuji, N., and Suemori, H. (2008). Recombinant human laminin isoforms can support the undifferentiated growth of human embryonic stem cells. Biochem. Biophys. Res. Commun. *375*, 27–32.

Miyazaki, T., Futaki, S., Suemori, H., Taniguchi, Y., Yamada, M., Kawasaki, M., Hayashi, M., Kumagai, H., Nakatsuji, N., Sekiguchi, K., and Kawase, E. (2012). Laminin E8 fragments support efficient adhesion and expansion of dissociated human pluripotent stem cells. Nat. Commun. *3*, 1236.

Morrison, S.J., Csete, M., Groves, A.K., Melega, W., Wold, B., and Anderson, D.J. (2000). Culture in reduced levels of oxygen promotes clonogenic sympathoadrenal differentiation by isolated neural crest stem cells. J. Neurosci. *20*, 7370–7376.

Musah, S., Wrighton, P.J., Zaltsman, Y., Zhong, X., Zorn, S., Parlato, M.B., Hsiao, C., Palecek, S.P., Chang, Q., Murphy, W.L., and Kiessling, L.L. (2014). Substratum-induced differentiation of human pluripotent stem cells

reveals the coactivator YAP is a potent regulator of neuronal specification. Proc. Natl. Acad. Sci. USA *111*, 13805–13810.

Nguyen, N.M., and Senior, R.M. (2006). Laminin isoforms and lung development: all isoforms are not equal. Dev. Biol. *294*, 271–279.

Nishiuchi, R., Takagi, J., Hayashi, M., Ido, H., Yagi, Y., Sanzen, N., Tsuji, T., Yamada, M., and Sekiguchi, K. (2006). Ligand-binding specificities of laminin-binding integrins: a comprehensive survey of laminin-integrin interactions using recombinant alpha3beta1, alpha6beta1, alpha7beta1 and alpha6beta4 integrins. Matrix Biol. *25*, 189–197.

Ohgushi, M., Minaguchi, M., and Sasai, Y. (2015). Rho-signaling-directed YAP/TAZ activity underlies the long-term survival and expansion of human embryonic stem cells. Cell Stem Cell *17*, 448–461.

Ohta, R., Niwa, A., Taniguchi, Y., Suzuki, N.M., Toga, J., Yagi, E., Saiki, N., Nishinaka-Arai, Y., Okada, C., Watanabe, A., et al. (2016). Laminin-guided highly efficient endothelial commitment from human pluripotent stem cells. Sci. Rep. *6*, 35680.

Pinco, K.A., Liu, S., and Yang, J.T. (2001). alpha4 integrin is expressed in a subset of cranial neural crest cells and in epicardial progenitor cells during early mouse development. Mech. Dev. *100*, 99–103.

Pryzhkova, M.V., Aria, I., Cheng, Q., Harris, G.M., Zan, X., Gharib, M., and Jabbarzadeh, E. (2014). Carbon nanotube-based substrates for modulation of human pluripotent stem cell fate. Biomaterials *35*, 5098–5109.

Przybyla, L., Lakins, J.N., and Weaver, V.M. (2016). Tissue mechanics orchestrate Wnt-dependent human embryonic stem cell differentiation. Cell Stem Cell *19*, 462–475.

Qin, P., Piechocki, M., Lu, S., and Kurpakus, M.A. (1997). Localization of basement membrane-associated protein isoforms during development of the ocular surface of mouse eye. Dev. Dyn. *209*, 367–376.

Rodin, S., Domogatskaya, A., Ström, S., Hansson, E.M., Chien, K.R., Inzunza, J., Hovatta, O., and Tryggvason, K. (2010). Long-term self-renewal of human pluripotent stem cells on human recombinant laminin-511. Nat. Biotechnol. *28*, 611–615.

Rodin, S., Antonsson, L., Niaudet, C., Simonson, O.E., Salmela, E., Hansson, E.M., Domogatskaya, A., Xiao, Z., Damdimopoulou, P., Sheikhi, M., et al. (2014). Clonal culturing of human embryonic stem cells on laminin-521/E-cadherin matrix in defined and xeno-free environment. Nat. Commun. *5*, 3195.

Sansores-Garcia, L., Bossuyt, W., Wada, K., Yonemura, S., Tao, C., Sasaki, H., and Halder, G. (2011). Modulating F-actin organization induces organ growth by affecting the Hippo pathway. EMBO J. *30*, 2325–2335.

Straight, A.F., Cheung, A., Limouze, J., Chen, I., Westwood, N.J., Sellers, J.R., and Mitchison, T.J. (2003). Dissecting temporal and spatial control of cytokinesis with a myosin II Inhibitor. Science *299*, 1743–1747.

Sun, Y., Yong, K.M., Villa-Diaz, L.G., Zhang, X., Chen, W., Philson, R., Weng, S., Xu, H., Krebsbach, P.H., and Fu, J. (2014). Hippo/YAP-mediated rigidity-dependent motor neuron differentiation of human pluripotent stem cells. Nat. Mater. *13*, 599–604.

Takahashi, K., Tanabe, K., Ohnuki, M., Narita, M., Ichisaka, T., Tomoda, K., and Yamanaka, S. (2007). Induction of pluripotent stem cells from adult human fibroblasts by defined factors. Cell *131*, 861–872.

Takayama, K., Nagamoto, Y., Mimura, N., Tashiro, K., Sakurai, F., Tachibana, M., Hayakawa, T., Kawabata, K., and Mizuguchi, H. (2013). Long-term self-renewal of human ES/iPS-derived hepatoblast-like cells on human laminin 111-coated dishes. Stem Cell Reports *1*, 322–335.

Takayama, K., Mitani, S., Nagamoto, Y., Sakurai, F., Tachibana, M., Taniguchi, Y., Sekiguchi, K., and Mizuguchi, H. (2016). Laminin 411 and 511 promote the cholangiocyte differentiation of human induced pluripotent stem cells. Biochem. Biophys. Res. Commun. *474*, 91–96.

Taniguchi, Y., Ido, H., Sanzen, N., Hayashi, M., Sato-Nishiuchi, R., Futaki, S., and Sekiguchi, K. (2009). The C-terminal region of laminin beta chains modulates the integrin binding affinities of laminins. J. Biol. Chem. *284*, 7820–7831.

Thomson, J.A., Itskovitz-Eldor, J., Shapiro, S.S., Waknitz, M.A., Swiergiel, J.J., Marshall, V.S., and Jones, J.M. (1998). Embryonic stem cell lines derived from human blastocysts. Science *282*, 1145–1147.

Toh, Y.C., Xing, J., and Yu, H. (2015). Modulation of integrin and E-cadherin-mediated adhesions to spatially control heterogeneity in human pluripotent stem cell differentiation. Biomaterials *50*, 87–97.

Xu, C., Inokuma, M.S., Denham, J., Golds, K., Kundu, P., Gold, J.D., and Carpenter, M.K. (2001). Feeder-free growth of undifferentiated human embryonic stem cells. Nat. Biotechnol. *19*, 971–974.

Yamada, M., and Sekiguchi, K. (2015). Molecular basis of laminin-integrin interactions. Curr. Top. Membr. *76*, 197–229.

Yu, J., Vodyanik, M.A., Smuga-Otto, K., Antosiewicz-Bourget, J., Frane, J.L., Tian, S., Nie, J., Jonsdottir, G.A., Ruotti, V., Stewart, R., et al. (2007). Induced pluripotent stem cell lines derived from human somatic cells. Science *318*, 1917–1920.

Zhao, B., Wei, X., Li, W., Udan, R.S., Yang, Q., Kim, J., Xie, J., Ikenoue, T., Yu, J., Li, L., et al. (2007). Inactivation of YAP oncoprotein by the Hippo pathway is involved in cell contact inhibition and tissue growth control. Genes Dev. *21*, 2747–2761.

STAR★METHODS

KEY RESOURCES TABLE

REAGENT or RESOURCE	SOURCE	IDENTIFIER
Antibodies		
Mouse anti-p75	Advanced Targeting Systems	Cat#AB-N07; RRID:AB_171797
Goat anti-SOX10	Santa Cruz Biotechnology	Cat#sc-17342; RRID:AB_2195374
Rabbit anti-TUBB3	Sigma-Aldrich	Cat#T2200; RRID:AB_262133
Mouse anti-E-cadherin	R&D Systems	Cat#MAB1838; RRID:AB_2076806
Goat anti-VSX2 (CHX10)	Santa Cruz Biotechnology	Cat#sc-21690; RRID:AB_2216006
Rabbit anti-PAX6	Covance Research Products Inc	Cat#PRB-278P; RRID:AB_291612
Mouse anti-MUC16	Abcam	Cat#ab697; RRID:AB_305676
Mouse anti-PITX2	Abcam	Cat#ab55599; RRID:AB_944836
Rabbit anti-FoxC1	Cell Signaling Technology	Cat#8758S
Mouse anti-p63	Santa Cruz Biotechnology	Cat#sc-8431; RRID:AB_628091
Rabbit anti-Myosin light chain (phosphor S20)	Abcam	Cat#ab2480; RRID:AB_303094
Rabbit anti-N-cadherin	Abcam	Cat#ab76011; AB_1310479
Goat anti-N-cadherin	Santa Cruz Biotechnology	Cat#sc-31030; RRID:AB_2077520
Mouse anti-YAP	Santa Cruz Biotechnology	Cat#sc-101199; RRID:AB_1131430
Rabbit anti-NANOG	Abcam	Cat#ab109250; RRID:AB_10863442
Mouse anti-TRA-1-60 Alexa Fluor 488 conjugate	BD Biosciences	Cat#560173; RRID:AB_1645379
Donkey anti-mouse IgG Alexa Fluor 488 conjugate	Life Technologies	Cat#A-21202; RRID:AB_141607
Donkey anti-mouse IgG Alexa Fluor 568 conjugate	Life Technologies	Cat#A-10037; RRID:AB_2534013
Donkey anti-rabbit IgG Alexa Fluor 488 conjugate	Life Technologies	Cat#A-21206; RRID:AB_141708
Donkey anti-rabbit IgG Alexa Fluor 594 conjugate	Life Technologies	Cat#A-21207; RRID:AB_141637
Donkey anti-goat IgG Alexa Fluor 488 conjugate	Life Technologies	Cat#A-11055; RRID:AB_2534102
Donkey anti-goat IgG Alexa Fluor 568 conjugate	Life Technologies	Cat#A-11057; RRID:AB_142581
Mouse anti-SSEA-4 PE conjugate	BioLegend	Cat#330406; RRID:AB_1089206
Mouse anti-CD104 Alexa Fluor 647 conjugate	BD PharMingen	Cat#624024
Mouse anti-CD200 PE-Cy7 conjugate	BD PharMingen	Cat#624052
Mouse anti-CD271 (p75) PE conjugate	BD Biosciences	Cat#557196; RRID:AB_396599
Mouse anti-CD49d (integrin α) APC conjugate	BioLegend	Cat#304308; RRID:AB_2130041
Rabbit anti-Lamin B1	Abcam	Cat#ab16048; RRID:AB_443298
Mouse anti-Vinculin	Abcam	Cat#ab18058; RRID:AB_444215
Rabbit anti-Vinculin (phosphoTyr822)	Sigma-Aldrich	Cat#V4889; RRID:AB_477624
Mouse anti-GAPDH	Abcam	Cat#ab8245; RRID:AB_2107448
Goat anti-Mouse IgG HRP conjugate	Abcam	Cat#ab6789; RRID:AB_955439
Goat anti-Rabbit IgG HRP conjugate	Abcam	Cat#ab97051; RRID:AB_10679369
Rat anti-mouse laminin α1 (5B7-H1)	(Manabe et al., 2008)	N/A
Rat anti-mouse laminin α2 (4H8-2)	(Manabe et al., 2008)	N/A
Rat anti-mouse laminin α3A (M35-N3-B9)	(Manabe et al., 2008)	N/A
Rat anti-mouse laminin α4 (M49-N7)	(Manabe et al., 2008)	N/A
Rat anti-mouse laminin α5 (M5N8-C8)	(Manabe et al., 2008)	N/A
Donkey Anti-Rat IgG Alexa Fluor 488	Abcam	Cat#ab150153; RRID:AB_2737355
Chemicals, Peptides, and Recombinant Proteins		
Y-27632	Wako	Cat#034-24024
CHIR99021	Sigma-Aldrich	Cat#SML1046-5MG
Verteporfin	Sigma-Aldrich	Cat#SML0534-5MG

(*Continued on next page*)

Continued

REAGENT or RESOURCE	SOURCE	IDENTIFIER
Blebbistatin	Wako	Cat#021-17041
Recombinant E8 fragments of laminin-111	(Taniguchi et al., 2009)	N/A
Recombinant E8 fragments of laminin-211	(Taniguchi et al., 2009)	N/A
Recombinant E8 fragments of laminin-332	(Miyazaki et al., 2012)	N/A
Recombinant E8 fragments of laminin-411	(Ohta et al., 2016)	N/A
Recombinant E8 fragments of laminin-511	(Ido et al., 2004, 2007; Taniguchi et al., 2009)	N/A
iMatrix-511 (LN511E8)	Nippi	Cat#892012
Recombinant Human KGF	Wako	Cat#112-00813
Knockout serum replacement (KSR)	Life Technologies	Cat#10828-028
Sodium pyruvate	Life Technologies	Cat#11360-070
Non-essential amino acids	Life Technologies	Cat#11140-050
Penicillin-streptomycin	Life Technologies	Cat#15140-122
2-Mercaptoethanol	Life Technologies	Cat#21985-023
Monothioglycerol	Wako	Cat# 195-15791
B27 supplement	Life Technologies	Cat#17504-044
4% (wt/vol) Paraformaldehyde (PFA) phosphate buffer solution	Wako	Cat# 163-20145
Normal donkey serum	Jackson ImmunoResearch	Cat#017-000-121
Hoechst 33342	Wako	Cat#346-07951
CytoPainter Phalloidin-iFluor 647 Reagent	Abcam	Cat#ab176759
Accutase	Life Technologies	Cat#A11105-01
Mitomycin C (Medicine)	Kyowa Hakko Kirin	N/A
FBS	Life Technologies	Cat#12483-020
Rhodamine B	Wako	Cat#180-00132
Dispase	Life Technologies	Cat#17105-041
Tissue-Tek OCT compound	Sakura finetek Japan	Cat#4583
Protease inhibitor cocktail	Wako	Cat#165-26021
PhosSTOP	Sigma-Aldrich	Cat#4906845001
5-bromo-4-chloro-3-indolyl phosphate (BCIP)/Nitro Blue Tetrazolium (NBT)	Sigma-Aldrich	Cat#11681451001
Critical Commercial Assays		
SuperScript III First-Strand Synthesis System for qRT-PCR	Life Technologies	Cat#18080051
NE-PER Nuclear and Cytoplasmic Extraction Reagents kit	Thermo Fisher Scientific	Cat#78833
Pierce BCA Protein Assay Kit	Thermo Fisher Scientific	Cat#23227
ECL Prime reagent	GE Healthcare	Cat#RPN2236
Cell Counting Kit-8	Dojindo	Cat#CK04
G-actin/F-actin *in vivo* Assay Biochem Kit	Cytoskelton	Cat#BK037
Deposited Data		
Microarray data	This paper	GEO: GSE116591
Experimental Models: Cell Lines		
Human: iPS cell line 201B7	RIKEN Bio Resource Center	Cat#HPS0063; RRID:CVCL_A324
Human: iPS cell line 1383D2	Center for iPS Cell Research and Application	N/A
Mouse: NIH 3T3 cell line	N/A	N/A
Oligonucleotides		
Taqman probes are listed in Table S2	Life Technologies	Cat#4331182

(*Continued on next page*)

Continued

REAGENT or RESOURCE	SOURCE	IDENTIFIER
Software and Algorithms		
GeneSpring GX v14.8	Agilent Technologies	RRID:SCR_010972; (https://www.agilent.com/en/product/cgh-cgh-snp-microarray-platform/cgh-cgh-snp-microarray-software)
StatLight 2000	Yukms	https://www.yukms.com/yukms/jap/html/StatLight/stalgt_jp.htm
FlowJo Ver v10.1	FlowJo, LLC	RRID:SCR_008520; (https://www.flowjo.com/solutions/flowjo)
SH800 v1-2	SONY	https://www.sonybiotechnology.com/us/
Image Lab Software v4.1	Bio-Rad	RRID:SCR_014210; (http://www.bio-rad.com/en-us/sku/1709690-image-lab-software?ID=1709690)

CONTACT FOR REAGENT AND RESOURCE SHARING

Further information and requests for resources and reagents should be directed to and will be fulfilled by the Lead Contact, Ryuhei Hayashi (ryuhei.hayashi@ophthal.med.osaka-u.ac.jp).

EXPERIMENTAL MODEL AND SUBJECT DETAILS

Animals

Pregnant female mice (C57/BL6; 10–16 weeks old; embryonic days [E] 12.5, E15.5, and E18.5) were acquired from SLC Japan (Shizuoka, Japan) for analysis of embryonic eyes. Animal experimentation was approved by the animal ethics committee of Osaka University.

Cell lines

hiPSC lines 201B7 and 1383D2 were obtained from the RIKEN Bio Resource Center (Tsukuba, Japan) and the Center for iPS Cell Research and Application (Kyoto University), respectively. hiPSCs were maintained on LN511E8 (0.5 $\mu g \cdot cm^{-2}$), prepared or purchased from Nippi (iMatrix-511, Tokyo, Japan), along with StemFit® medium (Ajinomoto, Tokyo, Japan) in a humidified 5% CO2 and 95% air atmosphere at 37°C. All experiments using recombinant DNA in this study were approved and conducted according to the regulations of the Recombinant DNA Committees of Osaka University. Mouse NIH 3T3 cell line was maintained with 10% FBS containing D-MEM (Life Technologies, Carlsbad, CA, USA) in a humidified 5% CO2 and 95% air atmosphere at 37°C. For use as feeder cells of colony formation assay, NIH 3T3 cells were treated with 8 $\mu g \cdot ml^{-1}$ mitomycin C for 2 h.

METHOD DETAILS

Immunohistochemical analyses

Frozen sections generated at E12.5, E15.5, and E18.5 were cut, air-dried, and incubated with TBS containing 5% donkey serum and 0.3% Triton X-100 (Sigma-Aldrich, St. Louis, MO, USA) for 1 h. Sections were then incubated with primary rat antibodies specific to laminin α1 (5B7-H1), laminin α2 (4H8-2), laminin α3A (M35-N3-B9), laminin α4 (M49-N7), or laminin α5 (M5N8-C8) (Manabe et al., 2008) for 3 h at room temperature or overnight at 4°C, followed by Alexa Fluor®-conjugated secondary antibodies (Life Technologies), and Hoechst 33342 stain (Molecular Probes, Eugene, OR, USA). Stained samples were observed using Axio Observer D1 (Carl Zeiss, Jena, Germany) and LSM 710 (Carl Zeiss) microscopes. Details of the antibodies used are listed in the Mouse Basement Membrane Bodymap (http://dbarchive.biosciencedbc.jp/archive/matrixome/bm/home.html).

Coating of culture plates

Coating of recombinant laminin E8 fragments (Ido et al., 2004, 2007; Taniguchi et al., 2009) was carried out by adding phosphate buffered saline (PBS) to culture plates and then adding laminin E8 fragments at a density of 0.5–1.5 $\mu g \cdot cm^{-2}$. Plates were incubated at 37°C for at least 1 h.

Ocular cell differentiation

The differentiation protocol used for the induction of hiPSCs into an eye-like SEAM was based on our previous reports (Hayashi et al., 2016, 2017) and is illustrated in Figure 1A. hiPSCs were seeded on dishes coated with five different isoforms of LNE8 and cultured in

StemFit® medium for 10 days. After hiPSC culture, the growth medium was switched to differentiation medium (DM). After 4 weeks, the medium was switched to corneal differentiation medium (CDM) and the cells cultured for an additional 4 weeks. At the beginning of week 9, the medium was replaced with corneal epithelium maintenance medium (CEM), in which the cells were grown for 4 weeks. Manual pipetting to remove non-epithelial-like cells, as carried out previously (Hayashi et al., 2016, 2017), was not performed in the present study. An Axio Observer D1 microscope (Carl Zeiss) was used to acquire phase contrast images. The composition of the medium used is as follows. DM; GMEM (Life Technologies, Carlsbad, CA, USA) supplemented with 10% knockout serum replacement (KSR; Life Technologies), 1 mM sodium pyruvate (Life Technologies), 0.1 mM non-essential amino acids (Life Technologies), 2 mM L-glutamine (Life Technologies), 1% penicillin-streptomycin solution (Life Technologies) and 55 μM 2-mercaptoethanol (Life Technologies) or monothioglycerol (Wako, Osaka, Japan), CDM; DM and CnT-20 or CnT-PR (without EGF or FGF2) (1:1, CELLnTEC Advanced Cell Systems, Bern, Switzerland) containing 20 ng·ml^{-1} KGF (Wako), 10 μM Y-27632 (Wako) and 1% penicillin-streptomycin solution, CEM; DMEM/F12 (1:1), (Life Technologies) containing 2% B27 supplement (Life Technologies), 1% penicillin-streptomycin solution, 20 ng·mL^{-1} KGF and 10 μM Y-27632.

Immunofluorescence staining

Cells were fixed with 4% paraformaldehyde (PFA), washed three times with Tris-buffered saline (TBS) (TaKaRa Bio, Shiga, Japan), and incubated with TBS containing 5% donkey serum and 0.3% Triton X-100 (Sigma-Aldrich) for 1 h to block non-specific reactions. They were then incubated with various primary antibodies (see Key Resources Table) overnight at 4°C and stained with Alexa Fluor®-conjugated secondary antibodies (Life Technologies) and Hoechst 33342 (Wako). Stained samples were observed using an Axio Observer D1 and LSM710 (Carl Zeiss).

qRT-PCR

Total RNA was extracted from cells using QIAzol reagent (QIAGEN, Venlo, Netherlands). SuperScript III First-Strand Synthesis System for qRT-PCR (Life Technologies) was used to synthesize cDNA. qRT-PCR was performed using an ABI Prism 7500 Fast Sequence Detection System (Life Technologies), according to the manufacturer's instructions. The TaqMan® MGB used is described in Table S2.

Flow cytometry and cell sorting

Cells differentiated from hiPSCs were dissociated using Accutase (Life Technologies) and stained with antibodies against SSEA-4 (330406, BioLegend, San Diego, CA, USA), CD104 (ITGB4; 624024, BD Biosciences, Franklin Lakes, NJ, USA), and CD200 (624052, BD Biosciences), as well as against CD271 (p75; 557196, BD Biosciences) and CD40d (ITGA4; 304308, BioLegend) as neural crest markers, for 30–60 min on ice. FACS Verse (BD Biosciences) or SH800 (Sony, Tokyo, Japan) was used for the analysis, and cell sorting was performed using an SH800 device. Data were analyzed using Sony SH800 and FlowJo software (TreeStar, San Carlos, CA, USA).

Colony formation assay

Sorted cells were seeded onto MMC-treated NIH 3T3 feeder cells at a density of 1000–2000 cells per 12-well plate and cultured in CMM (corneal epithelium maturation medium; KCM medium containing 20 ng·mL^{-1} KGF and 10 μM Y-27632) for 7–14 days. The colonies were fixed with 10% formaldehyde in neutral buffer solution, stained with rhodamine B (Wako), and counted to calculate the colony-forming efficiency.

Fabrication and harvesting of hiPSC-derived iCEC sheets

Preparation of hiPSC-derived iCEC sheets was performed based on a previously described protocol (Hayashi et al., 2016, 2017). iCECs obtained by FACS sorting were seeded onto 12-well plate or cell culture insert (BD Falcon, Bedford, MA, USA) and cultured in CEM until confluence. For harvesting, iCEC sheets were treated with 2.4 units·mL^{-1} Dispase (Life Technologies) at 37°C for 10 min, removed, and embedded in Tissue-Tek OCT compound (Sakura Finetek, Tokyo, Japan) and frozen. When cell culture insert is used, cell sheet on membrane was cut out and embedded.

Microarray analysis

Total RNA was isolated from differentiated hiPSCs (clone 201B7) grown on laminin isoforms on day 3 using an RNeasy Plus micro kit (QIAGEN). Microarray analysis using Sure Print G3 human 8 × 60K slides (Agilent Technologies, Palo Alto, CA, USA) was performed by TaKaRa Bio. The raw intensity values were imported into GeneSpring GX software (Agilent Technologies). The values were $\log_2$-transformed to the median of all samples and normalized to the 75th percentile. Principal component analysis, hierarchical clustering analysis, and pathway analysis using Wikipathways were performed using GeneSpring GX.

Time-lapse recording

For time-lapse recording, hiPSCs were visualized using an IncuCyte Live-Cell Imaging System (ESSEN BioScience Inc., Ann Arbor, MI, USA).

Quantification of hiPSC-derived colony diameters

The diameters of hiPSC colonies were measured using an EVOS FL Auto microscope and the accompanying software (Life Technologies).

Quantification of cell density within hiPSC colonies

Images of cells stained with Hoechst 33342 were acquired using an Axio Observer D1 microscope. The numbers of cells within a 100-μm square were manually counted from the images and converted into cells·mm^{-2}.

Cell fractionation and western blotting

Cells were lysed in RIPA buffer (Thermo Fisher Scientific, Waltham, MA, USA) containing protease inhibitor cocktail (Wako) and phosSTOP (Roche, Basel, Switzerland) according to the manufacturer's protocol. Nuclear and cytoplasmic fractions were prepared using the NE-PER Nuclear and Cytoplasmic Extraction Reagents kit (Thermo Fisher Scientific) according to the manufacturer's protocol. Protein concentrations were determined using a Pierce BCA Protein Assay Kit (Thermo Fisher Scientific). Equal amounts of protein were subjected to SDS-PAGE using NuPAGE 4%–12% gradient Bis-Tris gels, and transferred to polyvinylidene fluoride membranes using an iBlot system (Invitrogen, Waltham, MA, USA). The membrane was incubated with antibodies against YAP (sc-101199, 1:200, Santa Cruz Biotechnology), lamin B1 (ab16048, 1:10,000, Abcam, Cambridge, UK), p-MLC (ab2480, 1:1000; Abcam), p-vinculin (V4889, 1:1,000; Sigma-Aldrich), vinculin (ab18058; Abcam), or GAPDH (ab8245, 1:5,000; Abcam) for 3 h at room temperature or overnight at 4°C. After washing, membranes were incubated with horseradish peroxidase-conjugated anti-mouse IgG (ab6789, 1:5,000; Abcam) or anti-rabbit IgG (ab97051, 1:5,000; Abcam) secondary antibodies for 1 h at room temperature. Proteins were detected with ECL Prime reagent (GE Healthcare, Little Chalfont, UK), scanned, and analyzed with a ChemiDoc XRS+ imaging system and Image Lab software (Bio-Rad, Hercules, CA, USA).

Cell viability assay

Cell viability was measured using a Cell Counting Kit-8 (Dojindo, Kumamoto, Japan), according to the manufacturer's instructions. Absorbance was measured in a multilabel counter (ARVO MX, Perkin Elimer, MA, USA).

Alkaline phosphatase staining

Cells were washed with alkaline phosphatase buffer [100 mM Tris-HCl (pH 9.5) 100 mM NaCl, 5 mM $MgCl_2$] and stained with 5-bromo-4-chloro-3-indolyl phosphate/Nitro Blue Tetrazolium (BCIT/NBT) (Sigma-Aldrich) for 10 min. Cells were then rinsed twice with PBS and fixed with 4% PFA for 30 min and washed with deionized water. Observations were performed with an EVOS FL Auto system (Life Technologies).

Isolation of the cells in zone 1 of the SEAM

Cells from the central region on the colony (i.e., zone 1) were collected via pipetting. The cells were dissociated with Accutase for 1 h.

Assessment of F-actin/G-actin ratio

The status of F-actin/G-actin in hiPSCs grown on isoforms LN332E8 and LN511E8 on day 10 of culture was analyzed using a G-actin/F-actin *in vivo* assay kit (Cytoskelton, Inc., Denver, CO, USA), based on the manufacturer's protocol.

QUANTIFICATION AND STATISTICAL ANALYSIS

Statistical analysis

Statistical details of experiments described in corresponding figure legends. Data are represented as the mean ± standard error for each group. Statistical significance was analyzed via Student's t test, Tukey–Kramer test, Wilcoxon rank sum test, and Steel–Dwass test using StatLight 2000 software (Yukms Co. Ltd., Tokyo, Japan). All statistical analyses were conducted with a significance level of $\alpha = 0.05$ ($P < 0.05$).

DATA AND SOFTWARE AVAILABILITY

Microarray raw intensity values were imported into GeneSpring GX software ver 14.8 (Agilent Technologies). The accession number for the microarray data reported in this paper is Gene Expression Omnibus: GSE116591.